PASJ: Publ. Astron. Soc. Japan **60**, 85–93, 2008 February 25

Hot and Cool Plasmoid Ejections Associated with a Solar Flare

Masamitsu OHYAMA
Faculty of Education, Shiga University, 2-5-1 Hiratsu, Otsu, Shiga 520-0862
ohyama@sue.shiga-u.ac.jp
and
Kazunari SHIBATA
Kwasan and Hida Observatories, Kyoto University, Yamashina-ku, Kyoto 607-8471
shibata@kwasan.kyoto-u.ac.jp

(Received 2007 June 20; accepted 2007 September 11)

Abstract

A 1993 May 14 flare was associated with both X-ray plasma ejection as hot plasmoid ejection and Hα filament eruption as cool plasma ejection. The flare proceeded through two stages according to a GOES soft X-ray observation. In the first stage, an X-ray plasma ejection, an Hα filament eruption, and a chain of pointlike Hα brightenings occurred. In the second stage, an Hα two-ribbon flare and an X-ray arcade structure were seen in Hα and soft X-ray images, respectively. The X-ray plasmoid and the eruptive Hα filament were in the same current sheet. The X-ray plasmoid started to rise with a speed of $\sim 270\,\mathrm{km\,s^{-1}}$ temporally after the Hα filament eruption. The top part of the X-ray plasmoid moved together with the eruptive filament. They were then decelerated before the main peak of the hard X-ray emission. The X-ray plasmoid was not a bloblike feature, as the eruptive Hα filament, but a loop structure. Our results indicate that the X-ray plasmoid was not the heated part of the Hα filament.

Key words: Sun: activity — Sun: corona — Sun: filaments — Sun: flares — Sun: X-rays, gamma rays

1. Introduction

Some magnetic reconnection models, in which a reconnection in the vertical current sheet above flare loops is assumed to take place, were suggested as the two-ribbon flare model (e.g., Carmichael 1964; Sturrock 1966; Hirayama 1974; Kopp & Pneuman 1976; Forbes & Priest 1983; Moore & Roumeliotis 1992; Magara et al.1996; Yokoyama & Shibata 1997, 1998). These models are hereafter called CSHKP models. Moreover, Yohkoh discovered X-ray plasma ejections associated with not only long duration event (LDE) flares, such as two-ribbon flares, but also impulsive flares (e.g., Tsuneta 1993; Hudson 1994; Shibata et al.1995; Ohyama & Shibata 1997, 1998, 2000; Kim et al. 2004, 2005a, 2005b). On the basis of these observations, Shibata (1996, 1998) proposed a unified model, called a plasmoid-induced-reconnection model to explain impulsive flares, LDE flares, giant arcades associated with filament eruptions or colonal mass ejections (CMEs), and microflares in a unified scheme. In the model a plasmoid ejection plays a key role in inducing fast reconnection, and the ejected plasmoid (flux rope in 3D view) is a cool plasmoid as an Hα filament eruption and/or a hot plasmoid as X-ray plasma ejections.

The relation between Hα filament eruptions as cool plasmoid ejections and solar flares has been studied for a long time. Jing et al. (2004) examined filament eruptions using Hα data from 1999 to 2003, and found that 95% of active region filament eruptions were associated with flares. Sterling and Moore (2004a, 2004b) studied the earliest stages of quiet-region filament eruptions using EUV observations of SoHO and soft X-ray observations of Yohkoh. They found that eruptions began with a relatively slow rise of the filament (slow-rise phase), followed by a transition to a "fast-rise phase" of strong acceleration. In the case of an active-region filament eruption slow-rise phase and fast-rise phase were observed as quiet-region filament eruptions (Sterling & Moore 2005). The height-time profile of the observed filament (Sterling & Moore 2005) is qualitatively similar to that of the flux rope simulated by Chen and Shibata (2000) in which the reconnection between an emerging flux and another field under the flux rope triggers the eruption. Schuck et al. (2004) examined the temporal relationship between filament eruptions and soft X-ray emissions, and concluded that the filament eruption begins 2 hr before the first detectable enhancement in soft X-ray flux.

Yohkoh discovered X-ray plasma ejections as hot plasmoid ejections (e.g., Tsuneta 1993; Hudson 1994; Shibata et al.1995). Ohyama and Shibata (2000) examined limb flares between 1991 October and 1998 August and found that X-ray plasma ejections are seen in 63–70% of these flares. Moreover, they found that the occurrence rate increases with the flare strength as follows: 100% of the X-class flares, 74–82% of the M-class flares, and 31–38% of the C-class flares. It is difficult to detect X-ray plasma ejections in C-class flares, because the scale size and lifetime of ejections are short. Thus, they suggested that X-ray plasma ejections are general phenomena associated with solar flares. The relation between flares and X-ray plasma ejection by Ohyama and Shibata (2000) is similar to the relation between flares and CMEs (Yashiro et al. 2005). The velocity of X-ray plasma ejections is with the range of 30–$1300\,\mathrm{km\,s^{-1}}$ (Kim et al. 2005b). The X-ray plasmoid starts to be ejected slowly (at $10\,\mathrm{km\,s^{-1}}$) long before the impulsive phase (Ohyama & Shibata 1997). Then, the plasmoid is suddenly accelerated just before or at the onset of the impulsive phase, and thereafter decelerated or propagated at constant speed (Ohyama & Shibata 1997, 1998; Kim et al. 2005b). Time

evolutions of hot plasmoids as X-ray plasmoids are similar to the result of the numerically simulation (Magara et al. 1997), and are also similar to those of cool plasmoids as eruptive filaments and those of CMEs (Zhang et al. 2001).

Gopalswamy et al. (1997) examined a flare on 1994 July 31, which is associated with a prominence eruption and X-ray plasma ejection from radio to soft X-ray. They suggest that X-ray plasmoid seems to be the heated prominence. Grechnev et al. (2006) examined three eruptive prominences with two- and three-microwave data and images from EIT aboard SOHO. They found that no heating was observed on their main body, and proposed that the brightnings of eruptive prominences in EIT images were probably only due to heating of their thin envelopes. However, we do not yet well know the relationship between an X-ray plasmoid and an eruptive filament.

In this paper we analyze the 1993 May 14 flare, which was associated with both an X-ray plasma ejection and an Hα filament eruption. We examine the relationship between an X-ray plasmoid and an eruptive prominence.

2. Observations

An M4.4 class flare occurred on 1993 May 14 in the region NOAA 7500 at N20W48. The soft X-ray telescope (SXT) and the hard X-ray telescope (HXT) aboard Yohkoh observed this flare after 21:59 UT with the flare mode, although there was a data gap because of Yohkoh night. In this paper we use the soft X-ray images which were taken with the thick aluminum and beryllium filters to derive the physical parameters of the flare, such as the temperature, emission measure, pressure, and so forth. The Hα filtergram images of this flare were also available from the Big Bear Solar Observatory and National Astronomical Observatory of Japan. We used the magnetograms taken at Kitt Peak to coalign the SXT images with the Hα images.

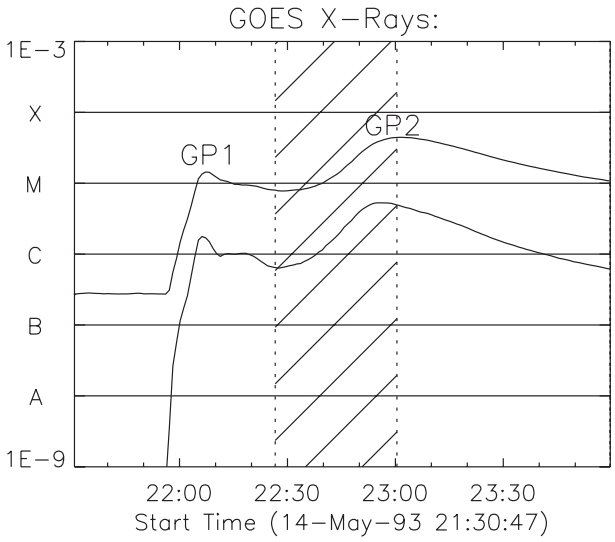

Fig. 1. Time profiles of the GOES X-ray intensity on 1993 May 14. The upper and lower curves indicate the full-sun soft X-ray flux through 1–8 Å and 0.5–4 Å, respectively. The shadow indicates the times when Yohkoh was hidden behind Earth. There are two peaks in this flare. The time of the first peak marked as GP1 is about 22:07 UT, and that of the second peak marked as GP2 is about 22:53 UT.

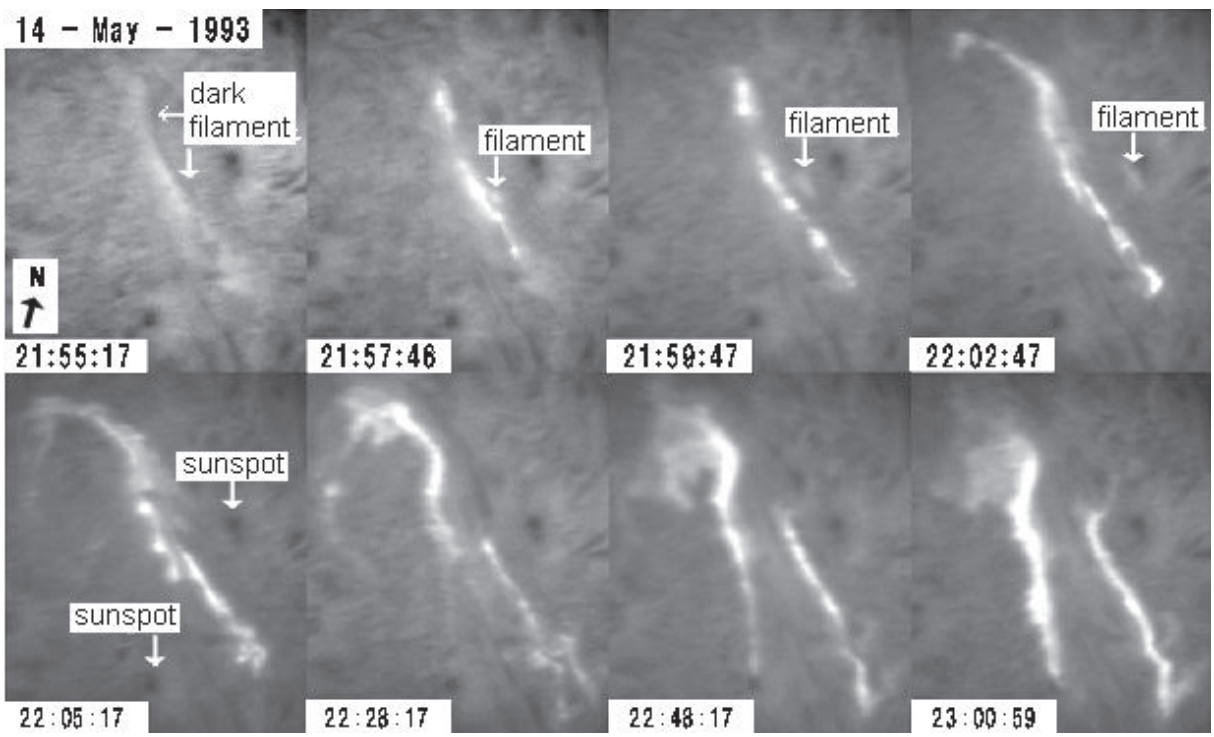

Fig. 2. Development of the flare on 1993 May 14. The eruptive filament is indicated by an arrow. The dark filament before its eruption is shown in 21:55:17 UT image.

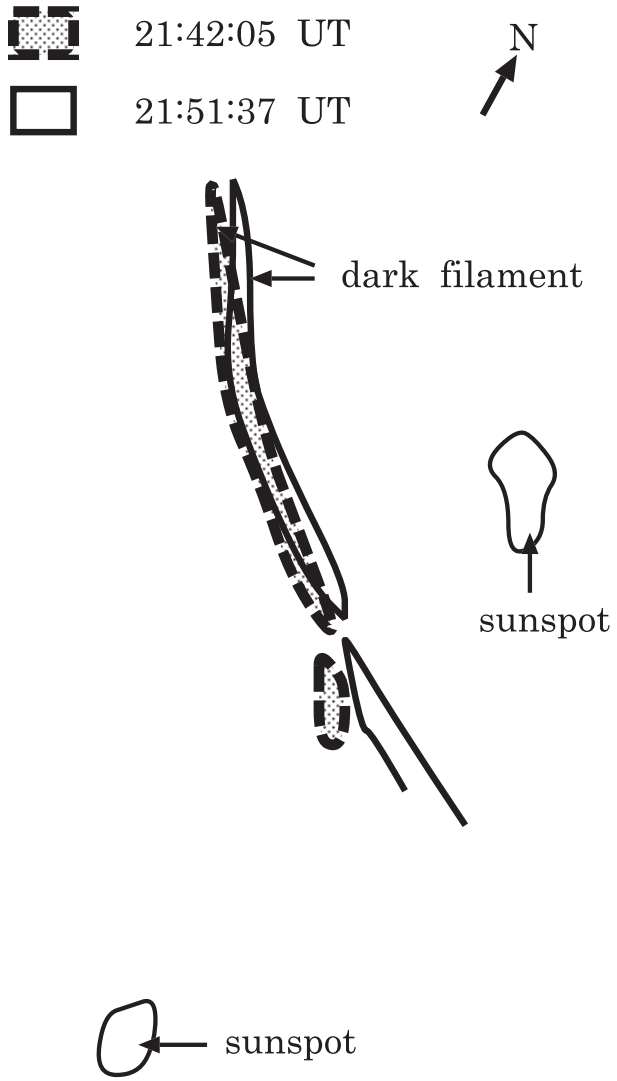

Fig. 3. Schematic picture of the dark filament before its eruption at 21:42:05 UT and 21:51:37 UT.

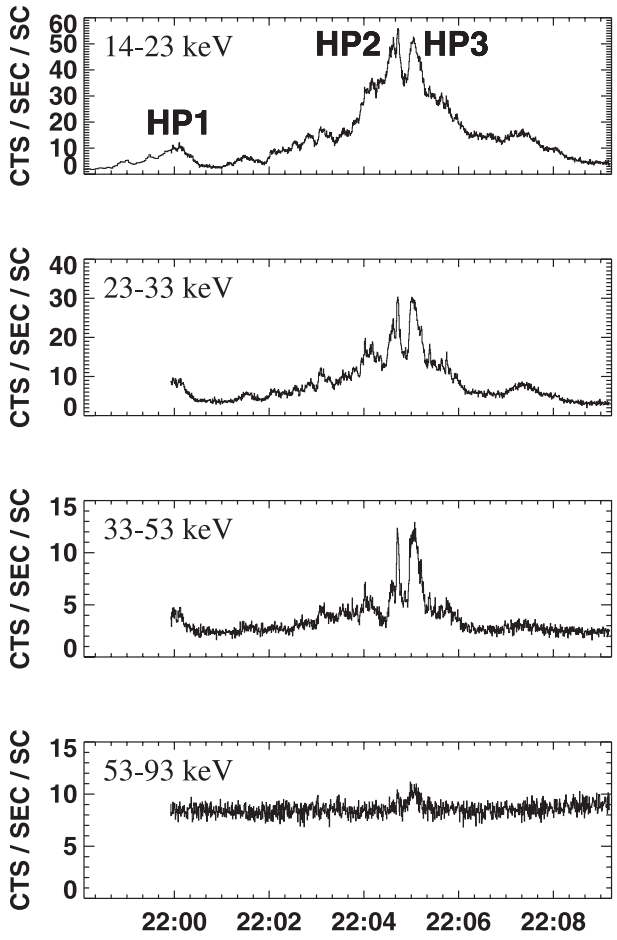

Fig. 4. Hard X-ray time profiles of the 1993 May 14 flare in the first stage. The intensities were measured in the four HXT energy bands in units of counts/sec/subcollimator. The times of the first, second, and third peaks marked as HP1, HP2, and HP3 are about 22:00:00, 22:04:40, and 22:05:00 UT, respectively.

3. Analysis and Results

3.1. Morphological Evolution

The flare, which was associated with both an Hα filament eruption and X-ray plasma ejection, occurred on 1993 May 14. The time profile of GOES X-ray flux is shown in figure 1. There were two peaks in this event; a first peak (GP1) at about 22:07, and a second (maximum) peak (GP2), corresponding to M4.4, at 22:53 UT. The duration of the first stage corresponding to GP1 was short, while that of the second stage corresponding to GP2 was long. Figure 2 shows the evolution of the flare observed in Hα. The second stage seemed to be simply a continuation of the first stage, and a gradual/decay phase of the first stage.

3.1.1. First stage

Figure 3 shows schematic images of the dark filament, which was an active-region filament in between sunspots, at 21:42:05 and 21:51:37 UT before the onset of the flare. The dark filament had already started to move westward, apparently before the onset of the flare, and the Hα enhancement started at about 21:54 UT. Figure 2 shows that a fragment of cool plasma (filament) apparently erupted westward. The erupted filament was not dark but bright and seemed to have originated from a patch of the dark filament or erupted from below the dark filament. Hα brightenings were composed of a chain of pointlike features, and spread both northeastward and southwestward with time (21:57:46–22:02:47 UT images in figure 2). The Hα brightenings separated into two ribbons from nearly their midpoint (22:02:47–23:00:59 UT). A bright arc lengthened from the north edge of the east ribbon (22:02:47–22:48:17 UT), and a bright blob fell near the arc (22:28:17 and 22:48:17 UT). Then, in the second stage a two-ribbon flare was clearly seen (22:48:17 and 23:00:59 UT). It is interesting that the filament eruption and point-like Hα brightenings were observed in the first stage, and that the two-ribbon flare appeared in the second stage.

SXT and HXT observed the first stage with the flare-mode since 21:59 UT. Figure 4 shows the hard X-ray time profile of the first stage detected with HXT. The hard X-ray emission of

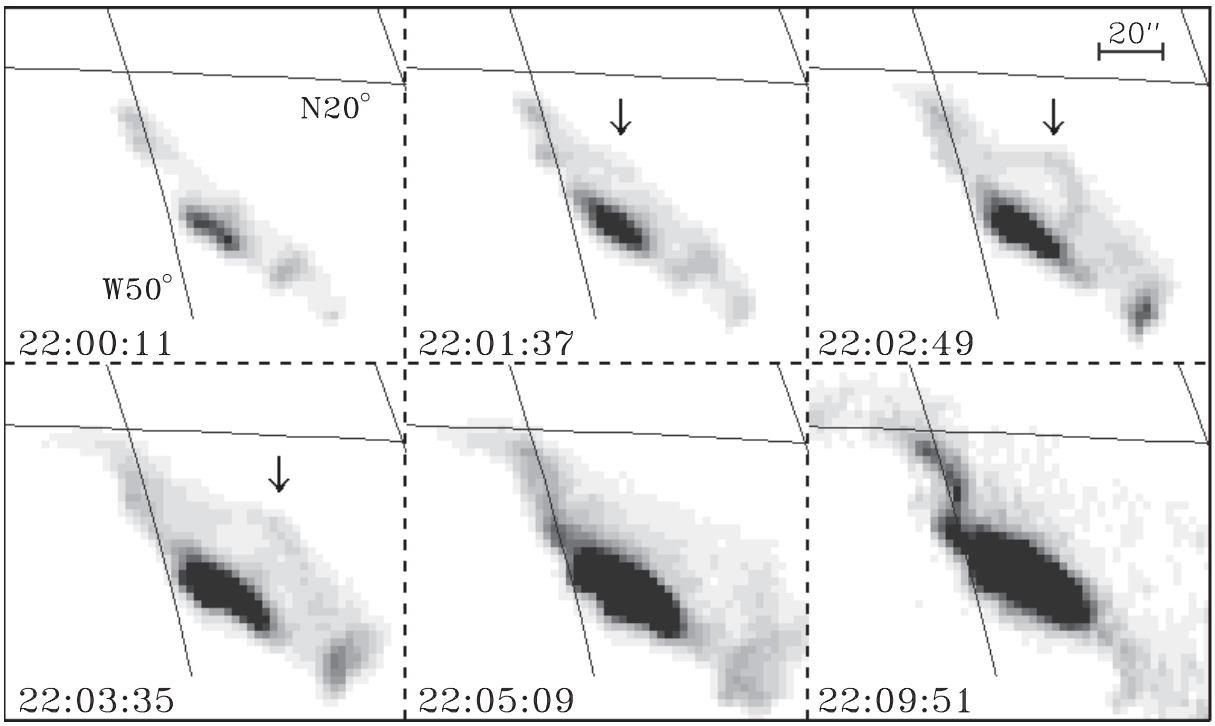

Fig. 5. Sequence of SXT images of the 1993 May 14 flare in the first stage. The X-ray plasmoid is indicated by an arrow. The longitudinal and lateral solid lines indicate N20 and W50, respectively.

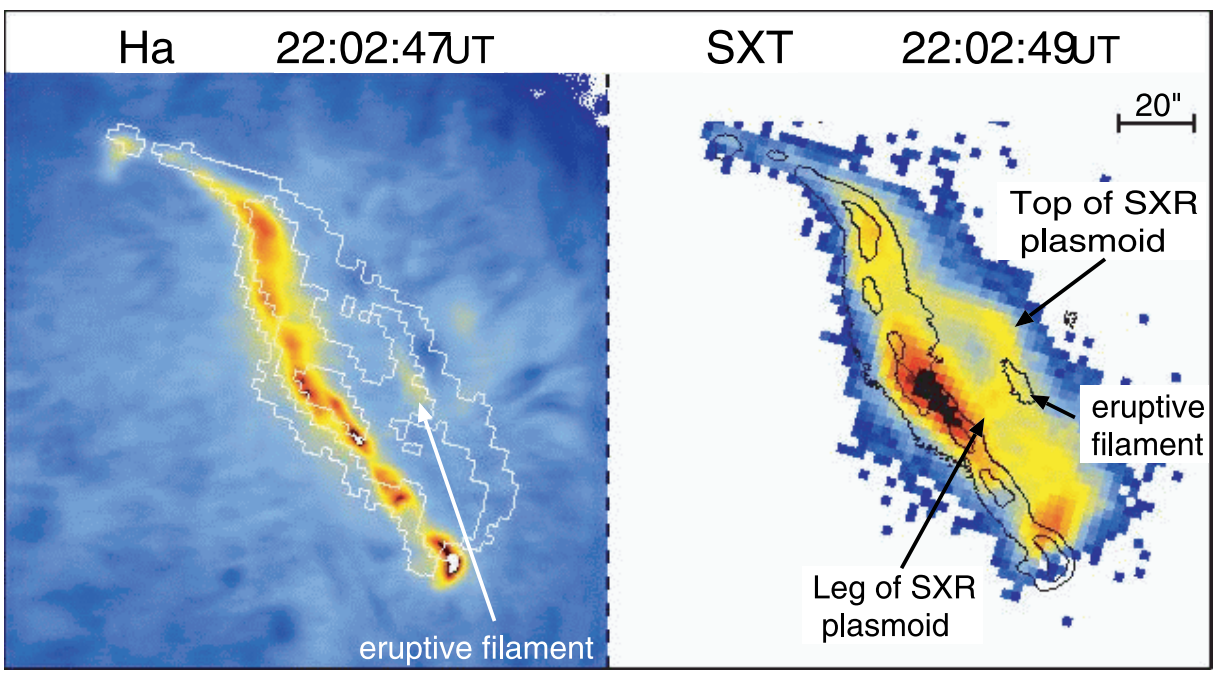

Fig. 6. Coalignment images between SXT and Hα images. (left) Contours of the SXT image overlaid on the Hα image. (right) Contours of the Hα image overlaid on the SXT image.

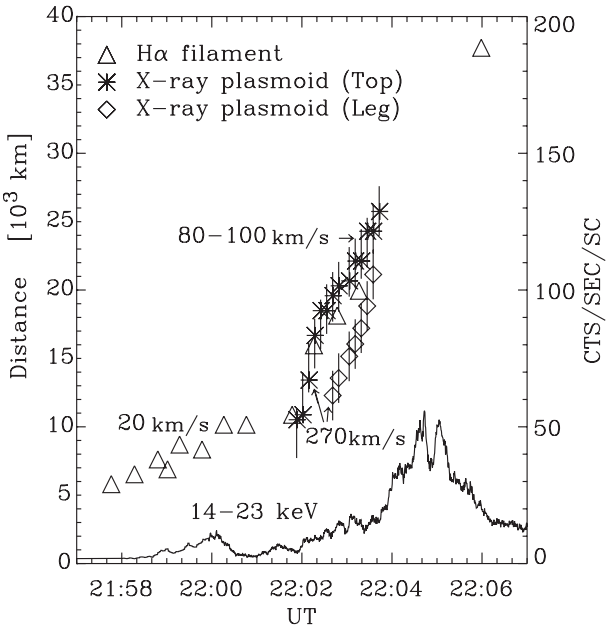

Fig. 7. Apparent displacement of the X-ray plasmoid and eruptive Hα filament for the 1993 May 14 flare. The bottom curve shows the counting rates from the 14–23 keV channel of HXT. Triangles indicate the height of the eruptive filament. Asterisks and diamonds indicate the top and leg of the X-ray plasmoid. The smooth curve of the eruptive filament is drawn from constant acceleration fits. The position of the leg of the X-ray plasmoid corresponds to that of the eruptive filament, if the X-ray plasmoid rises along nearly the same trajectory as the eruptive filament. The values of the velocity are the apparent velocity.

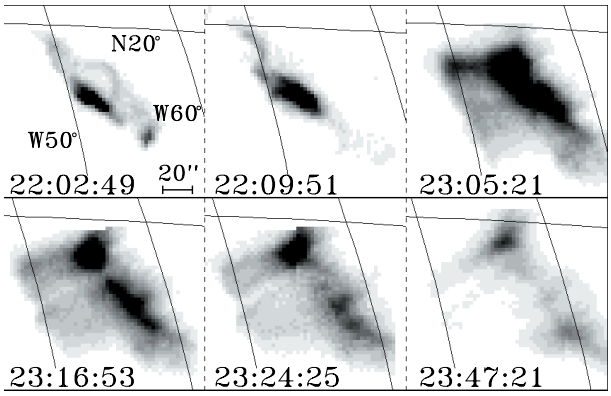

Fig. 8. Sequence of SXT images of the 1993 May 14 flare in the second stage. We also show SXT images (22:02:49 and 22:09:51 UT) of the first stage to make a comparison between the first and second stages.

the flare in the first stage began at about 21:58 UT and consisted of three peaks at about 22:00:00, 22:04:40, and 22:05:00 UT before the small peak of the GOES X-rays, GP1. We call these peaks HP1, HP2, and HP3, respectively. The intensity of HP1 was much weaker than those of HP2 and HP3, and those of HP2 and HP3 are nearly on a level. The soft X-ray evolution of the first stage is shown in figure 5. An X-ray loop structure which was hot plasmoid was ejected westward between HP1 and HP2. The loop shape of the ejected material is consistent with a three-dimensional view of a plasma ejection (i.e., plasmoid) in the reconnection model (e.g., Shibata et al. 1995). An X-ray arc structure, like the Hα arc, can be seen in the northeast of the flaring region.

We overlaid the Hα image on the SXT partial-frame image (PFI) to determine the spatial relation between the eruptive filament and the X-ray plasmoid. The process of coalignment between the Hα and SXT images is the following: (1) Coalignment between an SXT full-frame image (FFI) and a magnetogram (full sun) taken at Kitt Peak. (2) Coregistration between the SXT PFI and FFI images using the SXT aspect system. (3) Coalignment between the magnetogram and the Hα image using sunspots. (4) Coalignment between the Hα image and the SXT PFI image as the result of processes (1), (2), and (3). The coalignment accuracy is about 5″.

Figure 6 shows the Hα image at 22:02:47 UT coaligned with the SXT PFI image at 22:02:49 UT. The apparent features of the flare in the Hα and soft X-ray images are similar. The X-ray structures in the early phase of the filament eruption appeared nearly parallel to the pre-eruption filament, and the result is consistent with previous observations (Kahler 1981). The top part of the X-ray plasmoid was situated near the eruptive filament, though we do not know their positions along the direction of the line-of-sight. Figure 7 shows the apparent displacement of the eruptive filament and X-ray plasmoid without considering the projection effect. The Hα filament was ejected at $\sim 20\,\mathrm{km\,s^{-1}}$ ($\sim 30\,\mathrm{km\,s^{-1}}$ if we consider the projection effect assuming that the ejecta moved radially) before HP1 and was suddenly accelerated around 22:02 UT. (Note that if we define the impulsive phase for only HP2 and HP3, the acceleration occurred *before* the impulsive phase, whereas if the impulsive phase is defined as the period from the onset of HP1 to the end of HP3, then the acceleration occurred *during* the impulsive phase.)

On the other hand, the X-ray plasmoid was observed after HP1. Unfortunately, we could not determine the location where the X-ray plasmoid was launched, because the plasmoid was apparently hidden in the flaring loops in the early phase. The top part of the X-ray plasmoid moved together with the Hα filament with a projected speed of $\sim 270\,\mathrm{km\,s^{-1}}$ ($400\,\mathrm{km\,s^{-1}}$ considering the projection effect), and was decelerated to ~ 80–$100\,\mathrm{km\,s^{-1}}$ before the main peak of the hard X-ray emission, HP2. The speed after the deceleration was also similar to that of the eruptive filament.

3.1.2. Second stage

In the first stage the Hα brightenings were pointlike and aligned, and propagated both northeastward and southwestward with time. The Hα brightenings separated into two ribbons from nearly their midpoint during the transition phase between the first and second stages. The image in figure 2, taken at 22:28:17 UT, when the soft X-ray emission was nearly a minimum between GP1 and GP2, shows two Hα ribbons nearly aligned north–south. The distance between the two Hα ribbons increased, and the brightenings in the north (east) ribbon propagated southward to the sunspot. In the second stage the flare in Hα evolved into a typical two-ribbon flare (22:48:17 and 23:00:59 UT images in figure 2), and an X-ray arcade structure can be clearly seen in SXT images (figure 8).

Table 1. Physical parameters of the X-ray plasmoid and flare loops in the first stage (22:03:19 UT).

Physical parameter	Flare loops	X-ray plasmoid
Temperature (MK)	6.7–13.3	7.2–14.8 $(9.5 \pm 2.3)^*$
Emission measure (10^{28} cm^{-5})	17–393	6.2–55
Electron density (10^{10} cm^{-3})†	1.4–6.3	0.9–2.4
Gas pressure (dyn cm^{-2})	33–163	23–78
Mass (10^{14} g)	5.5 ± 0.2	~ 1.1
Thermal energy content (10^{29} erg)	~ 13	2.8 ± 0.2
Kinetic Energy (10^{28} erg)‡	—	0.5–10

* The value indicates the temperature at the center of the X-ray plasmoid.
† The line-of-sight length is taken to be 10^9 cm.
‡ The kinetic energy is estimated assuming that the derived mass is ejected with velocity 100–400 km s^{-1}.

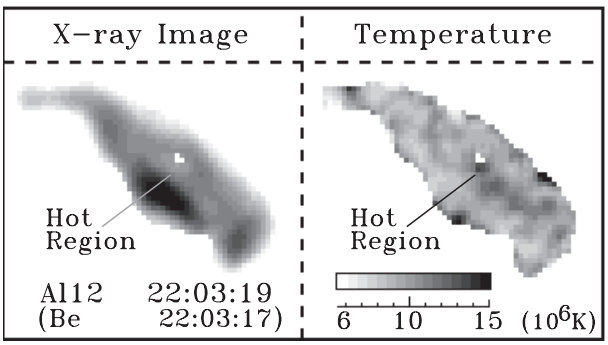

Fig. 9. X-ray intensity and temperature maps of the 1993 May 14 flare in the first stage. The X-ray image was taken with the thick aluminum filter at 22:03:19 UT. The temperature map was derived from the thick aluminum image, and the beryllium image taken at 22:03:17 UT. A hot region lies between the flare loops and the X-ray plasmoid.

3.2. Physical Conditions of X-Ray Plasmoid and Flare Loops

We derived the physical parameters of the flare of the first and the second stages from the SXT images using the filter-ratio method. The density, pressure, mass, and thermal energy content were calculated from the derived temperature and emission measure assuming a filling factor of unity and a line-of-sight length. Since the 1993 May 14 flare occurred on the solar disk, we assumed that the line-of-sight length is equal to the width of a loop for other limb flares, 10^9 cm.

3.2.1. First stage

We derived the physical parameters of the X-ray plasmoid and flare loops in the first stage after taking 3×3-pixel sums of the intensity in order to improve the statistics, because the plasmoid was transient in nature and its intensity was weak. Figure 9 shows the soft X-ray intensity and temperature maps of the flare in the first stage. It is found that a hot region, where the temperature was $\sim$ 12–14 MK, lies between the X-ray plasmoid and flare loops.

The physical parameters of the X-ray plasmoid and flare loops at 22:03:19 UT are summarized in table 1. The boundary of the X-ray plasmoid is defined as the place where the intensity is equal to $1/e^2 \sim 13.5\%$ of the maximum intensity in the X-ray plasmoid. By definition, the X-ray plasmoid includes a part of the hot region between the flare loops and the X-ray plasmoid, but it is difficult to identify the hot region as the bottom of the X-ray plasmoid, or as the outer region. If the hot region was a part of the X-ray plasmoid, the temperature of the X-ray plasmoid would have been 7.2–14.8 MK. If not, the temperature of the X-ray plasmoid was 9.5 ± 2.3 MK. The emission measure of the X-ray plasmoid was much smaller than that of the flare loop, but their temperatures were similar. The electron density of the X-ray plasmoid was $\sim (9-24) \times 10^9$ cm^{-3}, which is about an order of magnitude larger than the typical density of the active-region corona, 10^9 cm^{-3}. This is consistent with other X-ray plasma ejections (Ohyama & Shibata 1997, 1998). The mass of the X-ray plasmoid was $\sim 10^{14}$ g. The kinetic energy of the X-ray plasmoid was calculated using the estimated mass and a velocity of 100–400 km s^{-1}, and was $\sim (5-100) \times 10^{27}$ erg. The kinetic energy was smaller than its thermal energy content ($\sim 3 \times 10^{29}$ erg), while the latter was smaller than the thermal energy content of the flare loops, $\sim 10^{30}$ erg. Thus, the kinetic energy of the X-ray plasmoid was an order of magnitude smaller than the thermal energy content of the flare loops. This is also consistent with other X-ray plasma ejections (Ohyama & Shibata 1997, 1998).

3.2.2. Second stage

The physical parameters of flare loops in the second stage are summarized in table 2. They were derived after consecutive images were summed to obtain better statistics. Even the parameters of the first image were derived from X-ray images taken 15 min after the peak of GOES X-ray (GP2). The X-ray feature of each time is shown in figure 8.

The density, mass, and thermal energy content of the flare loops in the second stage were larger than those in the first stage. Even the temperature of the flare loops 15 min after GP2 was slightly hotter than that in the first stage.

4. Discussion

Both the Hα filament eruption and the X-ray plasma ejection occurred in the first stage. We are very interested in the spatial relation between two materials. Figure 6 shows that the top part of the X-ray plasmoid was situated near the eruptive filament, though we do not know their positions along the

Table 2. Physical parameters of flare loops in the second stage.

Time (UT)	Temperature (MK)	Density (10^{10} cm^{-3})	Pressure (dyn cm^{-2})	Mass (10^{15} g)	Thermal energy content (10^{30} erg)
23:05:03–23:09:53	7.1–15.3	2.3–11	52–262	~ 3	7.0 ± 0.1
23:10:01–23:13:57	7.1–14.2	2.3–11	53–251	~ 2.9	6.5 ± 0.1
23:14:03–23:18:57	7.2–13.8	2.3–10	55–234	~ 2.7	6.0 ± 0.1
23:19:03–23:25:45	6.7–12.0	2.3–9.2	50–211	~ 2.5	5.4 ± 0.1
23:30:01–23:53:45	6.6–10.7	2.3–7.1	50–146	~ 1.3	~ 2.7

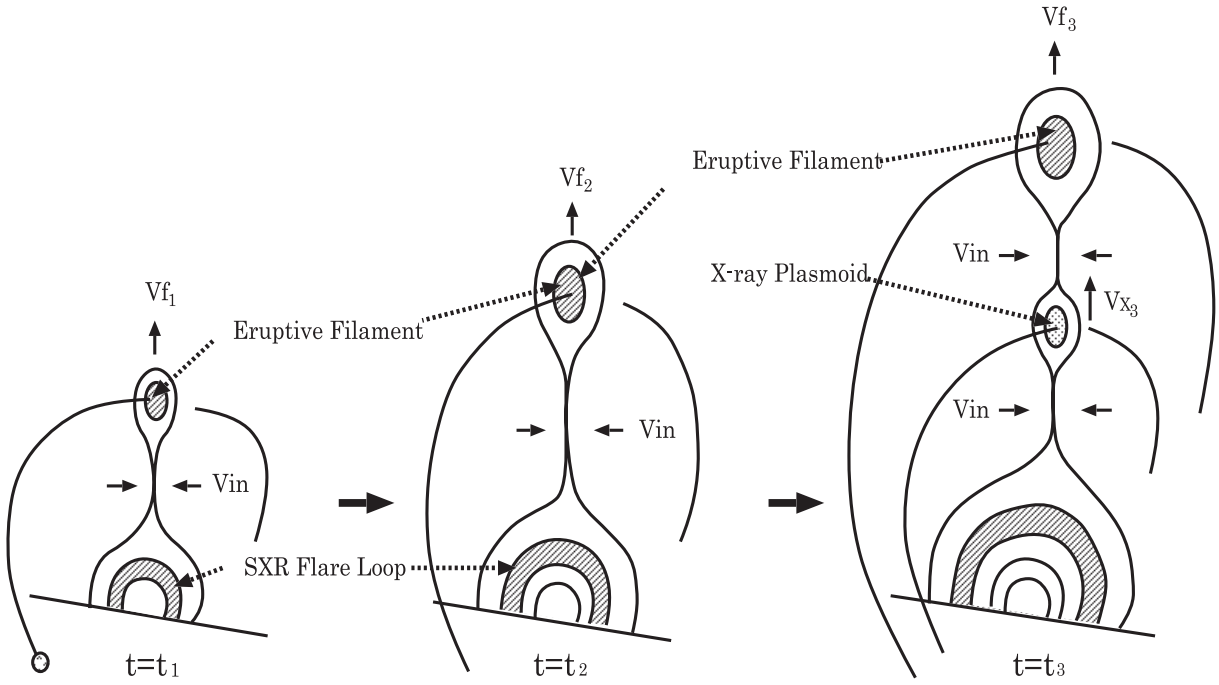

Fig. 10. Schematic picture of the magnetic reconnection model for the 1993 May 14 flare. This is an extension of the CSHKP model. $V_{\rm f}$ and $V_{\rm X}$ are the velocities of the eruptive filament and the X-ray plasmoid, respectively. $V_{\rm in}$ is the inflow speed to the reconnection point.

direction of the line-of-sight. X-ray plasmoid and eruptive Hα filament must be in a current sheet in order to be ejected, respectively. The observed Hα ribbon is magnetically linked to the erupting filament (figure 2). If the X-ray plasmoid were in another current sheet, other Hα brightenings (ribbons) corresponding to the X-ray plasmoid-related current sheet should be observed in Hα images. However, only a pair of ribbons was observed. Hence we suggest that the X-ray plasmoid and the eruptive filament were in the same current sheet, and that the top part of the X-ray plasmoid was located near the eruptive filament.

The top part of the X-ray plasmoid moved together with the eruptive Hα filament with a projected speed of 270 km s^{-1} between HP1 and HP2. They were decelerated to 80–100 km s^{-1} before the main peak of the hard X-ray emission, HP2 (figure 7). There is a possibility that hot plasmoid is formed by collisions between the reconnection jet and the flux rope (e.g., Shiota et al. 2005), because the X-ray plasmoid was accelerated and was near the Hα filament at the initiation of the X-ray plasmoid (figure 7). In this scenario the X-ray plasmoid may be a part of the filament heated by the collisions of the reconnection jet. However, the X-ray plasmoid was not a bloblike feature as the Hα filament, but a loop structure (figure 6). Moreover, the footpoint of the X-ray plasmoid seemed to connect with the surface, and the width of the X-ray plasmoid was the same as the Hα filament. It is thus difficult to think that all parts of the X-ray plasmoid were heated by the termination shock generated by the collision between the reconnecion jet and the flux rope. So we suggest that the X-ray plasmoid was not a part of the heated eruptive Hα filament.

We shall discuss how the observed results can be interpreted in terms of a reconnection model (figure 10). Suppose that magnetic reconnection may have occurred in a vertical current sheet between the eruptive filament and the flare loops ($t = t_1$). Since the eruptive Hα filament continued to rise, the current sheet may have lengthened further with the rise of the filament ($t = t_2$). Also suppose that an impulsive magnetic reconnection occurred once again somewhere in the current sheet ($t = t_3$). Since the material within the X-ray plasmoid, which was formed as secondary plasmoid(s) by the recent magnetic reconnection, would not include cool material, such as the Hα filament, and would be heated through slow shocks, or by the

reconnection jet, it could be observed in soft X-rays. Kliem, Karlický, and Benz (2000) and Karlický (2004) proposed that the secondary plasmoid is formed by the secondary tearing and subsequent coalescence processes. Karlický (2004) suggested that the slowly drifting structures in radio observations correspond to the radio emission from secondary plasmoids in the extended current sheet due to tearing and coalescence processes.

It will be necessary to investigate more flares associated with the simultaneous ejections of both X-ray plasma and Hα filament in order to know the relation between an X-ray plasmoid and an Hα filament.

Figure 7 shows that the slow-rise and fast-rise phases were observed for the Hα filament eruption, and that the fast-rise phase was associated with impulsive hard X-ray emission. This result is consistent with previous observational results (e.g., Ohyama & Shibata 1997, 1998; Sterling & Moore 2005; also two events reported in Kahler et al. 1988), and hence supports the model in which reconnection plays a crucial role in accelerating the filament/plasmoid ejection (e.g., Magara et al. 1997; Chen & Shibata 2000; Shibata & Tanuma 2001; Yokoyama & Shibata 2001). It should be noted, however, that the results of Kahler et al. (1988) suggest that at least in some events magnetic reconnection is only a secondary effect, suggesting other possibilities of filament acceleration, such as mass drainage (e.g., Low 2001) and MHD instabilities (e.g., Török & Kliem 2005).

5. Conclusion

A flare on 1993 May 14 proceeded through two stages. At the first stage both cool and hot plasmoid ejections occurred simultaneously. The cool plasmoid ejection was observed as a filament eruption by Hα observation of the Big Bear Solar Observatory, and the hot plasmoid ejection was observed as an X-ray plasma ejection by SXT aboard Yohkoh. The first stage also showed pointlike Hα brightenings, and the second stage showed an Hα two-ribbon flare and an X-ray arcade structure. The total released energy of the flare in the second stage was larger than that in the first stage.

We examined the physical condition of the X-ray plasmoid and the spatial relation between the X-ray plasmoid and eruptive Hα filament, and compared the total kinetic energy of the ejected plasma with the thermal energy content of the flare loops. The results are the following:

(1) The Hα filament had already started moving about 10 min before the onset of the impulsive phase of the first stage. The Hα filament was ejected at $20\,\mathrm{km\,s^{-1}}$ before, or at about the onset of, the impulsive phase, and was suddenly accelerated around 22:02UT.
(2) Before the main peak of the hard X-ray emission, but after the Hα filament eruption, the X-ray plasmoid was ejected at $\sim 270\,\mathrm{km\,s^{-1}}$. The top part of the X-ray plasmoid moved together with the eruptive filament, and they were decelerated to $\sim 100\,\mathrm{km\,s^{-1}}$.
(3) The X-ray plasmoid and eruptive Hα filament were in the same current sheet, because only a pair of ribbons were observed.
(4) The X-ray plasmoid was not a bloblike feature as the eruptive filament but a loop structure. Moreover, the footpoint of the X-ray plasmoid connected with the surface. Thus, the X-ray plasmoid was not a part of the heated eruptive filament.
(5) The temperature of the central region of the X-ray plasmoid loop was $9.5 \pm 2.3\,\mathrm{MK}$.
(6) The electron density of the X-ray plasmoid, $\sim (9-24) \times 10^9\,\mathrm{cm^{-3}}$, was an order of magnitude larger than that of a typical active-region corona.
(7) The masses of the X-ray plasmoid and eruptive Hα filament were estimated to be $\sim 10^{14}$ g and $\leq 10^{15}$ g, respectively.

We are grateful to Professor T. Sakurai and Drs. H. S. Hudson and A. Sterling for many useful comments on the manuscript. The authors are grateful to Professor H. Wang and Big Bear Solar Observatory for help with accessing the BBSO's Hα images. We would like to thank all of the Yohkoh team members. The Yohkoh mission is a project of the ISAS, Japan, with substantial participation from other institutions within Japan, and with important contributions from the research groups in the US and the UK under the support of NASA and SERC. This work was supported in part by a Grant-in-Aid for the 21st Century COE "Center for Diversity and Universality in Physics" from the Ministry of Education, Culture, Sports, Science and Technology (MEXT), and also in part by a Grant-in-Aid for Creative Scientific Research "The Basic Study of Space Weather Prediction" (Head Investigator: K. Shibata) from MEXT.

References

Carmichael, H. 1964, in Proc. AAS-NASA Symp. on the Physics of Solar Flares, ed. W. N. Hess (Washington, D.C.: NASA), 451
Chen, P. F., & Shibata, K. 2000, ApJ, 545, 524
Forbes, T. G., & Priest, E. R. 1983, Sol. Phys., 84, 169
Gopalswamy, N., Kundu, M. R., Manoharan, P. K., Raoult, A., Nitta, N., & Zarka, P. 1997, ApJ, 486, 1036
Grechnev, V. V., Uralov, A. M., Zandanov, V. G., Baranov, N. Y., & Shibasaki, K. 2006, ApJ, 58, 69
Hirayama, T. 1974, Sol. Phys., 34, 323
Hudson, H. S. 1994, in Proc. of Kofu Meeting, ed. S. Enome & T. Hirayama (Nagano: Nobeyama Radio Observatory), 1
Jing, J., Yurchyshyn, V. B., Yang, G., Xu, Y., & Wang, H. 2004, ApJ, 614, 1054
Kahler, S. W. 1981, Sol. Phys., 71, 337
Kahler, S. W., Moore, R. L., Kane, S. R., & Zirin, H. 1988, ApJ, 328, 824
Karlický, M. 2004, A&A, 417, 325
Kim, Y.-H., Moon, Y.-J., Cho, K.-S., Bong, S.-C., & Park, Y.-D. 2004, J. Korean Astron. Soc., 37, 171
Kim, Y.-H., Moon, Y.-J., Cho, K.-S., Bong, S.-C., & Park, Y. D. 2005b, ApJ, 635, 1291

Kim, Y.-H., Moon, Y.-J., Cho, K.-S., Kim, K.-S., & Park, Y. D. 2005a, ApJ, 622, 1240
Kliem, B., Karlický, M., & Benz, A. O. 2000, A&A, 360, 715
Kopp, R. A., & Pneuman, G. W. 1976, Sol. Phys., 50, 85
Low, B. C. 2001, J. Geophys. Res., 106, 25141
Magara, T., Mineshige, S., Yokoyama, T., & Shibata, K. 1996, ApJ, 466, 1054
Magara, T., Shibata, K., & Yokoyama, T. 1997, ApJ, 487, 437
Moore, R. L., & Roumeliotis, G. 1992, in Eruptive Solar Flares, ed. Z. Švestka, B. V. Jackson, & M. E. Machado (New York: Springer-Verlag), 69
Ohyama, M., & Shibata, K. 1997, PASJ, 49, 249
Ohyama, M., & Shibata, K. 1998, ApJ, 499, 934
Ohyama, M., & Shibata, K. 2000, J. Atmos. Sol.-Terr. Phys., 62, 1509
Schuck, P. W., Chen, J., Schwartz, I. B., & Yurchyshyn, V. 2004, ApJ, 610, L133
Shibata, K. 1998, in Solar Jets and Coronal Plumes, ed. T.-D. Guyenne (Noordwijk: ESA), 137
Shibata, K., Masuda, S., Shimojo, M., Hara, H., Yokoyama, T., Tsuneta, S., Kosugi, T., & Ogawara, Y. 1995, ApJ, 451, L83
Shibata, K., & Tanuma, S. 2001, Earth Planets Space, 53, 473
Shibata, K., Yokoyama, T., & Shimojo, M. 1996, Adv. Space Res., 17, 197
Shiota, D., Isobe, H., Chen, P. F., Yamamoto, T. T., Sakajiri, T., & Shibata, K. 2005, ApJ, 634, 663
Sterling, A. C., & Moore, R. L. 2004a, ApJ, 602, 1024
Sterling, A. C., & Moore, R. L. 2004b, ApJ, 613, 1221
Sterling, A. C., & Moore, R. L. 2005, ApJ, 630, 1148
Sturrock, P. A. 1966, Nature, 211, 695
Török, T., & Kliem, B. 2005, ApJ, 630, L97
Tsuneta, S. 1993, ASP Conf. Ser., 46, 239
Yashiro, S., Gopalswamy, N., Akiyama, S., Michalek, G., & Howard, R. A. 2005, J. Geophys. Res., 110, A12S05
Yokoyama, T., & Shibata, K. 1997, ApJ, 474, L61
Yokoyama, T., & Shibata, K. 1998, ApJ, 494, L113
Yokoyama, T., & Shibata, K. 2001, ApJ, 549, 1160
Zhang, J., Dere, K. P., Howard, R. A., Kundu, M. R., & White, S. M. 2001, ApJ, 559, 452